



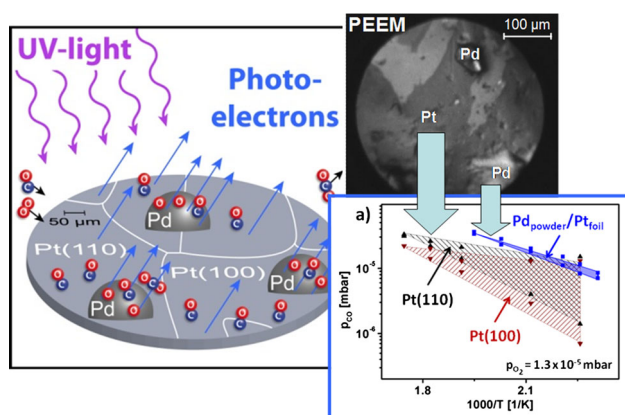
Analysing the Reaction Kinetics for Individual Catalytically Active Components: CO Oxidation on a Pd Powder Supported by Pt Foil

M. Datler · I. Bespalov · G. Rupprechter · Y. Suchorski

Received: 22 December 2014 / Accepted: 13 January 2015 / Published online: 11 March 2015
© The Author(s) 2015. This article is published with open access at Springerlink.com

Abstract Spatially- and component-resolved kinetic measurements and resulting phase diagrams for CO oxidation on a model catalyst consisting of Pd powder agglomerates supported by a polycrystalline Pt foil are reported. The kinetic data for the micrometer-sized Pt(100) and Pt(110) domains and for the different Pd powder agglomerates of similar dimensions were obtained by local analysis of PEEM video-sequences recorded in situ during the ongoing CO oxidation reaction. Individual domains of the supporting Pt foil as well as the μm -sized Pd powder agglomerates behave in the combined $\text{Pd}_{\text{powder}}/\text{Pt}_{\text{foil}}$ sample independently from each other with respect to CO oxidation, at least in the 10^{-5} mbar pressure range. The propagating reaction fronts move within grain boundaries for Pt domains and also remain confined to the Pd agglomerates.

Graphical Abstract



Keywords CO oxidation · Reaction kinetics · Photoemission electron microscopy · Heterogeneous catalysis · Kinetic transitions

1 Introduction

Modern technical catalysts used e.g. in automotive catalytic converters are typically multicomponent systems consisting of mixed metal oxides and different supported precious metals, such as Pt, Pd, Rh [1–3]. The resulting reaction kinetics appears to be quite complex due to the contributions of different individual catalytically active components and their complex interactions with the oxidic substrate [4, 5]. For a mechanistic understanding of the processes occurring in such complex systems and for theoretical modelling it would be important to differentiate between the individual active components. The usual mass-spectrometric detection of reaction products can hardly solve this task, since it does not distinguish between product species originating from different catalytically active surface sites. Simplified model systems whose different components are spatially separated by sub-mm distances may allow for the use of a “scanning-MS” with gas sampling via a capillary leak [6]. Nevertheless, as for every scanning procedure, parallel measurements for many different locations are not possible with this method. Additionally, the products from neighbouring locations might also attain the sampling nozzle-sniffer.

The problem of catalytic properties evaluation for spatially separated species on the same sample is in principle similar to that of individual domains of a heterogeneous surface. This task was recently solved, at least for CO oxidation on Pt and Pd, by the “kinetics by imaging” approach employing photoemission electron microscopy

M. Datler · I. Bespalov · G. Rupprechter · Y. Suchorski (✉)
Institute of Materials Chemistry, Vienna University of
Technology, Getreidemarkt 9, 1060 Vienna, Austria
e-mail: yuri.suchorski@tuwien.ac.at

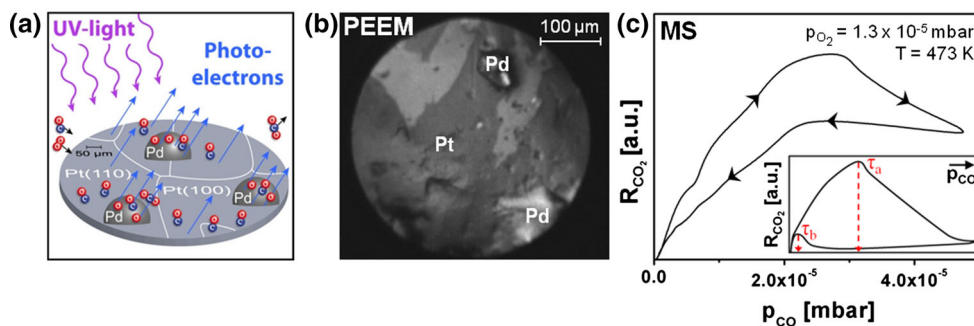


Fig. 1 PEEM studies on a combined Pd_{powder}/Pt_{foil} sample. **a** Idea of the experiment: photoelectrons emitted during CO oxidation and in situ collected by PEEM provide spatially- and component-resolved kinetic data; **b** PEEM image of the ongoing CO oxidation: Pd agglomerates and reaction fronts on the Pt surface are visible: whereas the dark Pt surface is catalytically active (oxygen covered), the bright Pt surface is inactive (CO poisoned), T = 473 K,

(PEEM, Fig. 1a) [7, 8]. The idea to use PEEM as a method for local kinetic measurements is based on the correlation of the PEEM intensity with catalytic activity, as observed earlier in averaging studies on Pt single crystal surfaces [9]. Extrapolated to the local measurements on individual domains of a polycrystalline Pt-foil, this idea allowed to pursue the kinetic transitions during the reaction and even to create local kinetic phase diagrams for individual crystalline grains [7, 8, 10, 11].

In the current contribution we extend this idea to $\mu\text{-m}$ sized Pd powder agglomerates supported by a polycrystalline Pt foil consisting of differently oriented domains (50–100 μm in size, Fig. 1b). Such a model system is well suitable for proving the possibility to study the reaction kinetics not only in a spatially-resolved but also in a component-distinctive way since the parameter ranges of catalytic activity for CO oxidation differ significantly for Pd and Pt [8]. In addition, the work function changes caused by CO and oxygen adsorption on Pt and Pd surfaces lead to differing contrasts in PEEM during the CO oxidation: an oxygen covered Pt surface appears as “dark” [7, 12] in contrary to the Pd surface [8, 13] which appears as “bright” upon oxygen adsorption. This allows an easy differentiation between the Pt support and Pd powder particles down to the resolution limit of the available PEEM (a few μm in our case).

2 Experimental

The experiments were performed in an all-metal UHV setup consisting of two separate chambers (PEEM and XPS) connected with each other by a sample transfer line, as described in detail elsewhere [14]. The PEEM chamber

$p_{\text{O}_2} = 1.3 \times 10^{-5}$ mbar, $p_{\text{CO}} = 1.8 \times 10^{-6}$ mbar; **c** total CO₂ production rate as measured by MS upon cyclic varying p_{CO} and at constant T = 473 K and $p_{\text{O}_2} = 1.3 \times 10^{-5}$ mbar. Kinetic transition points are not evident from the MS data due to the overlap of differing R_{CO₂} curves for Pt and Pd. The inset shows, for comparison, the corresponding curve for the Pt(111) surface with clearly visible τ_a and τ_b transition points, as adapted from Ref. [16]

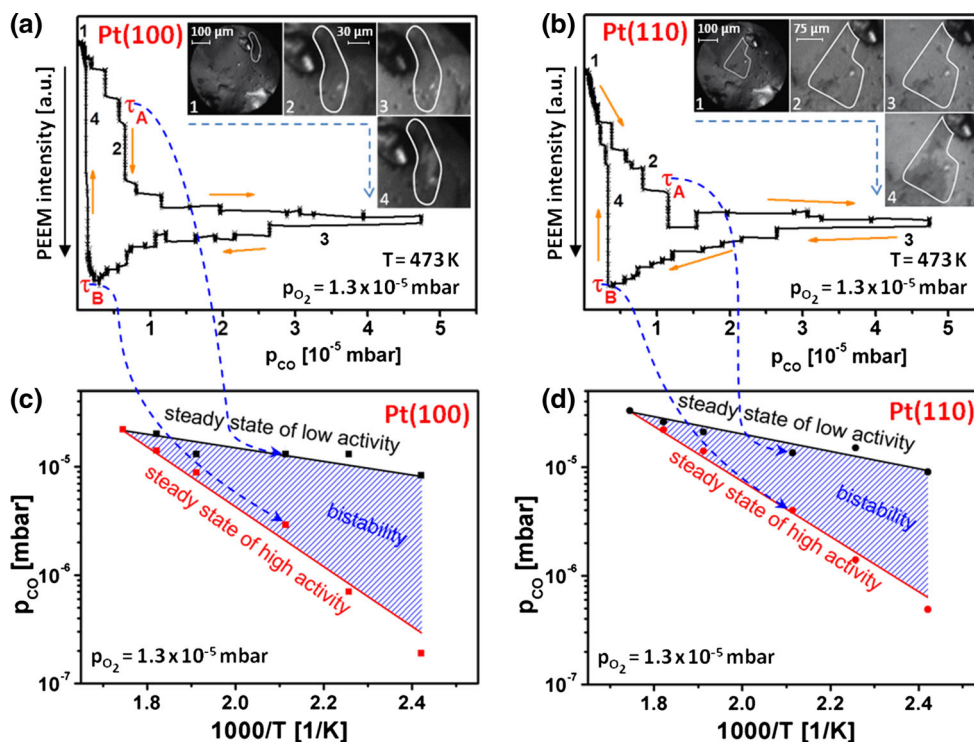
is equipped with a PEEM optics (Staib Instruments), a deuterium discharge UV lamp (photon energy ~ 6.5 eV) for electron excitation, a QMS (MKS Instruments), a gas supply system (O₂: 99.99 %, CO: 99.97 %) and sample preparation facilities for cleaning the sample by argon ion sputtering and subsequent annealing. The XPS chamber is equipped by a Phoibos 100 hemispherical energy analyzer and XR-50 twin anode X-ray source (SPECS) and independent sample preparation facilities. Differential pumping of the PEEM intensifier section by a separate turbomolecular pump and two in-line apertures along the photoelectron trajectory (diameter 4.0 and 0.3 mm) allow to keep the pressure inside the PEEM below 10^{-7} mbar, while the local pressure of reactants at the sample can be extended up to 10^{-4} mbar.

The PEEM chamber has been used as a flow reactor for CO oxidation, the PEEM images were recorded in situ by a high-speed CCD camera (Hamamatsu). The image magnification was calibrated by comparison of PEEM images with optical micrographs of the same sample region. The recorded PEEM video-sequences were related to MS-data obtained simultaneously by a quadrupole mass spectrometer (MKS) placed in the vicinity of the sample.

A PEEM image, formed by photoelectrons, represents the lateral distribution of the local work function across the Pd_{powder}/Pt_{foil} sample. This allows to distinguish between differently oriented grains of the Pt foil used as a support and the Pd powder agglomerates (Fig. 1b), as well as between different adsorbates by correlating local image intensities with the known work function values of the corresponding clean and adsorbate-covered Pt and Pd surface [7].

The combined Pd_{powder}/Pt_{foil} sample consisted of a 10×12 mm polished polycrystalline Pt foil of 0.2 mm

Fig. 2 PEEM monitoring of CO oxidation on the Pt support of the Pd_{powder}/Pt_{foil} sample. **a** Hysteresis-like plot of the local PEEM intensity of a Pt(100) domain during cyclic variation of the CO pressure at constant $T = 473$ K and $p_{O_2} = 1.3 \times 10^{-5}$ mbar; **b** the same for Pt(110). The insets show chosen PEEM frames for particular characteristic parts of the hysteresis loop; **c** local kinetic phase diagram for the Pt(100) domain, resulting from a series of hysteresis loops measured at different temperatures; **d** the same, but for the Pt(110) domain



thickness (Mateck, 99.99 %) and Pd powder (Mateck, 99.99 %) mechanically pressed into the supporting Pt foil. The sample was cleaned in UHV by repeated cycles of sputtering with Ar⁺ ions at 1 keV for 15 min at room temperature and consecutive annealing to 1073 K for 20 min. To remove carbonaceous segregation products contaminating the surface, the sample was repeatedly heated in oxygen at a partial oxygen pressure of 8×10^{-7} mbar at a temperature between 673 and 773 K. The cleanness of the sample was controlled by XPS, no Pt- or Pd-oxide formation was observed at present reaction conditions. The sample temperature was measured by a Ni/NiCr thermocouple spot-welded to the front side of the sample.

3 Results and Discussion

The kinetics of CO oxidation on a model system surface can be summarized by a so-called kinetic phase diagram, a chart in the T , p_{CO} , p_{O_2} parameter space, where the transition points between the steady states of high reactivity and low reactivity as well as the region of bistability are plotted [15, 16]. The reason to denote such a chart as a “phase diagram” lies in the formal similarities between the non-equilibrium kinetic transitions occurring in the reaction and equilibrium phase transitions: as already noticed by Schlögl in the 1970s, in both equilibrium and non-equilibrium phase transitions a crucial role is played by

cooperative phenomena forming, for example, ordered structures in an equilibrium, and self-organizing dissipative structures in a non-equilibrium situation [17, 18]. The role of the order parameter in the equilibrium phase transition is adopted, in case of reaction, by the coverage of the reactants, and the point where bistability sets in corresponds to the critical point (bifurcation) [19–21]. The transition points from high reactivity (oxygen covered surface) to low reactivity (CO poisoned surface) can be obtained by MS tracking the hysteresis-like CO₂ production rate (R_{CO_2} curve) at varying e.g. p_{CO} at constant p_{O_2} and T [7, 8, 15, 16].

In the case of a heterogeneous surface this approach meets its limits: the transitions points are often “smeared out” as observed e.g. for polycrystalline surfaces consisting of different domains [8], or are not detectable at all. Figure 1c illustrates this for the present Pd_{powder}/Pt_{foil} system: due to an overlap of the R_{CO_2} curves for Pt and Pd, which differ significantly [8], the resulting R_{CO_2} dependence does not exhibit distinct transition points. For comparison, the corresponding R_{CO_2} curve for a Pt(111) single crystal surface is shown as inset of Fig. 1c displaying pronounced transitions from the active to the inactive state and vice versa [16].

As already mentioned in the introduction, PEEM monitoring of the reaction might provide a solution in such case. In the present study, CO oxidation was monitored by PEEM, in parallel to the MS measurements illustrated in Fig. 1c.

Figure 2 shows the results of such monitoring, with the focus first being directed to two different domains of the supporting Pt foil, namely Pt(100) and Pt(110). To determine locally-resolved kinetics, the local PEEM intensity was integrated within a specific, selected domain, and plotted as a function of p_{CO} (Fig. 2a for a Pt(100) domain and 2b for a Pt(110) domain). The kinetic transitions appear as pronounced drops and jumps in the local PEEM intensity hysteresis curves measured during a cyclic variation of the CO pressure at constant $T = 473 \text{ K}$ and $p_{\text{O}_2} = 1.3 \times 10^{-5} \text{ mbar}$.

The sharp transition τ_A from the active steady state to inactive state results from suppression of oxygen adsorption by CO at increasing CO pressure and the reverse transition τ_B to the active state occurs as “reactivation” at decreasing CO pressure. However, the latter happens at much lower CO pressure than τ_A due to the known “asymmetry” of CO and oxygen adsorption (the oxygen molecule needs two neighbouring adsorption sites for dissociative adsorption) [9, 12]. Analogous measurements of a series of local hysteresis curves at different reaction temperatures then allowed to construct a local domain-specific phase diagram for (100) and (110) domains of the supporting Pt foil (Fig. 2c, d respectively). Other (100) and (110) domains on the Pt foil behaved identically, due to the identical gas pressure and temperature all over the sample. Similarly as in our earlier reports [7, 8], also in the current case the adjacent domains on the polycrystalline Pt foil behave independently in CO oxidation in the present range of CO and oxygen pressures, i.e. diffusional coupling is effectively inhibited by grain boundaries and the pressure variations are insufficient for gas-phase coupling [8].

As a parallel imaging technique, PEEM provides this type of information for the whole field of view at any reaction time [7] and thus this approach was applied to the two μm -sized Pd powder agglomerates visible in the Fig. 1b. The corresponding hysteresis curves measured at 473 K are shown in Fig. 3a, b where again the sharp kinetic transitions τ_A and τ_B are clearly visible. It should be noted that in PEEM the τ_A and τ_B transitions for the Pd agglomerates appear with “inverse contrast” with respect to Pt: the PEEM image of Pt becomes bright upon CO poisoning while that of Pd gets dark during the τ_A transition, since the work function of the CO covered Pd surface is higher than that of the same oxygen covered surface, in contrary to Pt where the work function of the CO covered surface is lower than that of oxygen covered [8]. As clearly seen from Fig. 3a, b, the behaviour of the two Pd agglomerates differing in size and shape, appears to be identical, at least with respect to the kinetic transitions τ_A and τ_B .

Similarly, as in the case of the supporting Pt foil, the local kinetic phase diagrams for the Pd agglomerates can be extracted from a series of local hysteresis curves at

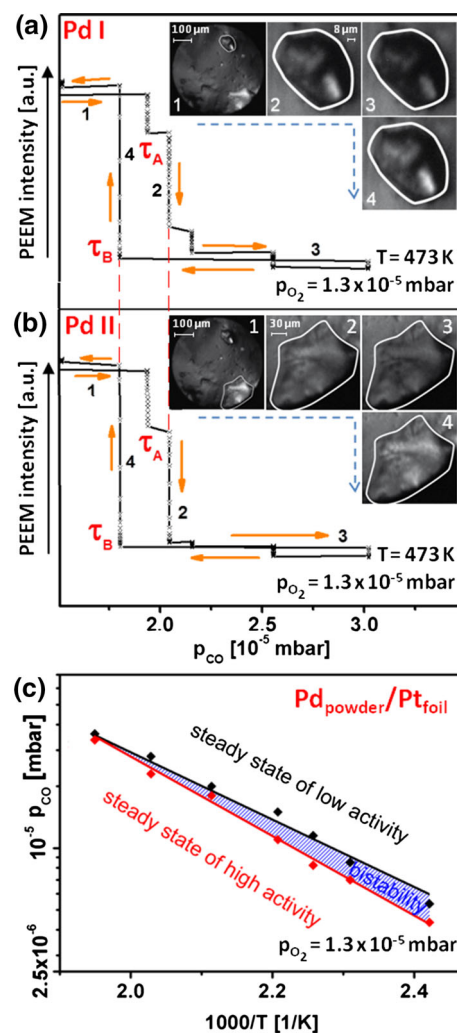


Fig. 3 Comparison of the catalytic behaviour of two Pd agglomerates visible in Fig. 1b. **a** Hysteresis-like PEEM intensity plots measured locally for the “upper” Pd agglomerate during cyclic variation of the CO pressure at constant temperature of 473 K and a constant partial oxygen pressure of $1.3 \times 10^{-5} \text{ mbar}$. The insets show chosen PEEM frames for particular characteristic parts of the hysteresis loop, the Pd agglomerate, corresponding to the hysteresis loop is marked by white line. Note the opposite direction of the intensity axis in comparison to Fig. 2; **b** the same, but for the “lower” Pd agglomerate; **c** local kinetic phase diagram for the Pd agglomerates

different reaction temperatures, for which the same PEEM video-sequences, which were exploited for construction of diagrams for Pt(100) and Pt(110) domains (Fig. 2 c, d), could be used. Figure 3c exhibits the results of the evaluation showing the common kinetic phase diagram for two Pd powder agglomerates, which behave identically.

The diagrams for the Pt(100) and the Pt(110) domains as well as a common diagram for the two Pd agglomerates are summarized in Fig. 4a. It should be noted that all three diagrams characterizing the different domains and different components are obtained in one experiment, i.e. at fully identical conditions and after the identical preparation

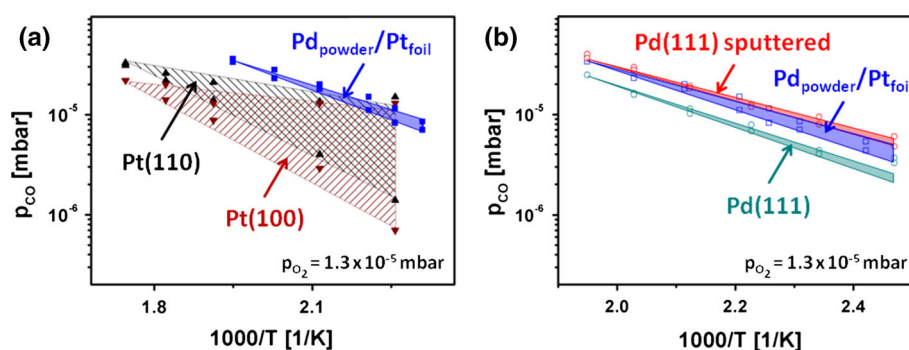


Fig. 4 Comparison of the kinetic phase diagrams for different components of the model sample. **a** diagrams for Pt(100) and Pt(110) domains of the supporting Pt foil from Fig. 2c, d in comparison with the diagram for the supported Pd agglomerates

procedure for all regions of the sample. The diagrams for Pt(100) and Pt(110) are in quantitative agreement with those measured for the corresponding Pt domains without Pd agglomerates [8] and with data for corresponding single crystal surfaces [12]. This means that also for a combined Pd_{powder}/Pt_{foil} sample the individual domains of the supporting Pt foil behave independently from each other, and from the Pd agglomerates.

It is interesting to compare the results for the Pd powder agglomerates with known data for different Pd surfaces. Figure 4b shows such a comparison of the current data with the Pd(111) surface [8], and with the same Pd(111) surface but after Ar⁺ ion bombardment, i.e. with an artificially defected surface [13]. The comparison shows that the reactive behaviour of the Pd agglomerates differs significantly from that of the smooth ordered Pd(111) domain, with the CO poisoning (upper boundary of the bistability region) occurring for Pd powder at a considerably higher CO partial pressure than for the smooth Pt(111) surface. Correspondingly, the Pd powder surface is also reactivated at a higher CO pressure than the ordered Pd(111) surface, i.e. the defect-rich Pd powder surface is much more tolerant toward CO poisoning than the smooth ordered surface.

The same effect is observed for the defect-rich Ar⁺ sputtered Pd surface: the diagrams for the Pd powder and for the Ar⁺ sputtered Pd(111) overlap in the Fig. 4b. Apparently, the degree of the surface disorder and the density of defects created by Ar⁺ sputtering is similar to that existing on the surface of Pd agglomerates in present study. STM observations of such Ar⁺ sputtered surfaces performed in our recent study showed that ion bombardment of the Pd surface leads to formation of three-dimensional islands, with a very high density of steps and edges [13]. The formed “mound”-like islands have uppermost terraces with the diameters of 2–3 nm, and the slope angles are between 10° and 20°, corresponding to

(from Fig. 3c); **b** the same diagram as in **a** for the supported Pd agglomerates in comparison with diagrams for the ordered Pd(111) surface and sputtered (highly defected) Pd(111) surface (the latter two adapted from Ref. [13])

terrace widths of 0.6–1.2 nm. This means that about one-quarter of all surface Pd atoms are step or kink atoms. One can imagine that present Pd powder agglomerates have a similarly high density of steps and edges with a considerably higher binding energy of oxygen than that of flat terraces [22].

Although the CO binding energy is also altered on such defect sites on the Pd surface [23], the impact on the CO adsorption kinetics appears to be rather small in the present case in comparison with that of oxygen. Since the kinetics of the competitive CO and oxygen coadsorption is governed by the energetics of adsorption, this explains why the Pd powder surface (and sputtered Pd) can withstand a higher CO pressure prior to being poisoned. The reverse transition τ_B occurs also at a higher CO-to-oxygen pressure ratio than on the smooth Pd: due to the high step and defect density of the powder (and sputtered) surface more favourable sites for oxygen adsorption are available, even on a mainly CO-covered surface, i.e. the higher sticking probability for oxygen adsorption forces an “earlier” reactivation.

In conclusion, it should be noted that the spatial resolution of the applied approach is solely limited by the resolution of the used PEEM, i.e. employing the best modern devices which resolution nears lower nm-range, the local kinetic analysis of individual catalytic particles in a commercial catalyst should be feasible.

4 Summary

We report area- and component-specific kinetic measurements and resulting phase diagrams for CO oxidation on a model catalyst, consisting of Pd powder agglomerates supported by a polycrystalline Pt foil. The kinetic data for the individual (100) and (110) domains of the Pt foil and for the different micrometer-sized Pd powder agglomerates

were obtained in a spatially-resolved way by local analysis of PEEM video-sequences recorded in situ during the ongoing reaction. Due to the parallel imaging principle of PEEM, the data were obtained simultaneously and at fully identical conditions for all regions and all components of the multicomponent model system.

In the combined Pd_{powder}/Pt_{foil} sample individual domains of the supporting Pt foil as well as the μm-sized Pd powder agglomerates behave independently from each other with respect to CO oxidation, at least in the 10⁻⁵ mbar pressure range. The propagating reaction fronts move within grain boundaries for Pt domains and also remain confined to the Pd agglomerates. Apparently, the micrometer-size of the domains and the low total pressure hinder the reactive synchronization via adsorbate diffusion or gas phase coupling, respectively. The spatial resolution of the used approach is limited solely by the resolution of the available PEEM.

Acknowledgments This work was supported by the Austrian Science Fund (FWF) [SFB F45 FOXSI]. Technical support by Johannes Frank (IMC, TU Vienna) is cordially acknowledged.

Open Access This article is distributed under the terms of the Creative Commons Attribution License which permits any use, distribution, and reproduction in any medium, provided the original author(s) and the source are credited.

References

1. Shelef M, McCabe RW (2000) *Catal Today* 62:35
2. Gandhi HS, Graham GW, McCabe RW (2003) *J Catal* 216:433
3. Farrauto RJ, Heck RM (1999) *Catal Today* 51:351
4. Happel M, Myslivec J, Johánek V, Dvorák F, Stetsovych O, Lykhach Y, Matolín V, Libuda J (2012) *J Catal* 289:118
5. Tingting Z, Junjun H, Yunkun Z, Wenzheng X, Jieli H (2014) *J Rare Earths* 32:97
6. Johansson M, Hoffmann Jørgensen J, Chorkendorff I (2004) *Rev Sci Instrum* 75:2082
7. Suchorski Y, Spiel C, Vogel D, Drachsel W, Schlögl R, Rupprechter G (2010) *Chem Phys Chem* 11:3231
8. Vogel D, Spiel C, Suchorski Y, Trincherro A, Schlögl R, Grönbeck H, Rupprechter G (2012) *Angew Chem Int Ed* 51:10041
9. Ertl G (1990) *Adv Cat* 37:213 and references therein
10. Vogel D, Spiel C, Suchorski Y, Urich A, Schlögl R, Rupprechter G (2011) *Surf Sci* 605:1999
11. Spiel Ch, Vogel D, Suchorski Y, Drachsel W, Schlögl R, Rupprechter G (2011) *Catal Lett* 141:625
12. Ertl G (2008) *Angew Chem Int Ed* 47:3524
13. Vogel D, Spiel C, Schmid M, Stöger-Pollach M, Schlögl R, Suchorski Y, Rupprechter G (2013) *J Phys Chem C* 117:12054
14. Vogel D, Budinska Z, Spiel C, Schlögl R, Suchorski Y, Rupprechter G (2013) *Catal Lett* 143:235
15. Berdau M, Yelenin G, Karpowicz A, Ehsasi M, Christmann K, Block JH (1999) *J Chem Phys* 110:11551
16. Suchorski Y, Wrobel R, Becker S, Weiss H (2008) *J Phys Chem C* 112:20012
17. Schlögl F (1971) *Z Phys* 248:446
18. Schlögl F (1972) *Z Phys* 253:147
19. Zhdanov VP, Kasemo B (1994) *Surf Sci Rep* 20:113
20. Bykov VI, Elokhin VI, Gorban AN, Yablonskii GS (1991) Kinetic models of catalytic reactions. In: *Comprehensive chemical kinetics*, vol. 32. Elsevier, Amsterdam *Comprehensive Chemical Kinetics*
21. Suchorski Y, Beben J, Imbihl R, James EW, Liu D-J, Evans JW (2001) *Phys Rev B* 63:165417
22. Zhang Y, Rogal J, Reuter K (2006) *Phys Rev B* 74:125414
23. Yudanov IV, Sahnoun R, Neyman KM, Rösch N, Hoffmann J, Schauerermann S, Johánek V, Unterhalt H, Rupprechter G, Libuda J, Freund HJ (2007) *J Phys Chem B* 107:255